ORIGINAL PAPERS

Radiationless deactivation pathways versus H-atom elimination from the N–H bond photodissociation in $PhNH_2$-$(Py)_n$ ($n = 1,2$) complexes

Mounir Esboui[1] · Jalloul Trabelsi[2]

Abstract

Minimum energy structures of the ground and lowest excited states of aniline ($PhNH_2$) solvated by pyridine (Py) show that the clusters formed are stabilized by hydrogen bonds in which only one or both hydrogen atoms of the NH_2 group take part. Two different N–H bonds photodissociation in $PhNH_2$-$(Py)_n$ ($n = 1,2$) complexes, free and hydrogen bonded have been studied by analyzing excited state potential energy surfaces. In the first one, only N–H bonds engaged in hydrogen bonding in these complexes are considered. RICC2 calculations of potential energy (PE) profiles indicate that all photochemical reaction paths along N–H stretching occur mainly via the proton-coupled electron transfer (PCET) mechanism. The repulsive charge transfer $^1\pi\pi^*$(CT) state dominates the PE profiles, leading to low-lying $^1\pi\pi^*$(CT)/S_0 conical intersections and thus provide channels for ultrafast radiationless deactivation of the electronic excitation or stabilization to biradical complexes. The second photoreaction consists of a direct dissociation along the free N–H bond of the NH_2 group. It has been shown that this process is played by excited singlet states of $^1\pi\sigma^*$ character having repulsive potential energy profiles with respect to the stretching of N–H bond, which dissociates over an exit barrier about 0.5 eV giving rise to the formation of a $^1\pi\sigma^*$/S_0 conical intersection. This may cause an internal conversion to the ground state or may lead to H-atom elimination. This photophysical process is the same in both planar and T-shaped conformers of the $PhNH_2$-Py monomer complex. Our findings reveal that there is no single dominating path in the photodissociation of N–H bonds in $PhNH_2$-$(Py)_n$ complexes, but rather a variety of paths involving H-atom elimination and several quenching mechanisms.

✉ Mounir Esboui
mounir.esboui@fst.rnu.tn

1 LSAMA, Department of Physics, Faculty of Sciences, University of Tunis El-Manar, 2092 Tunis, Tunisia

2 High Institute of Environmental Sciences and Technologies of Borj Cedria, University of Carthage, Tunis, Tunisia

Graphical abstract

N-H photodissociation
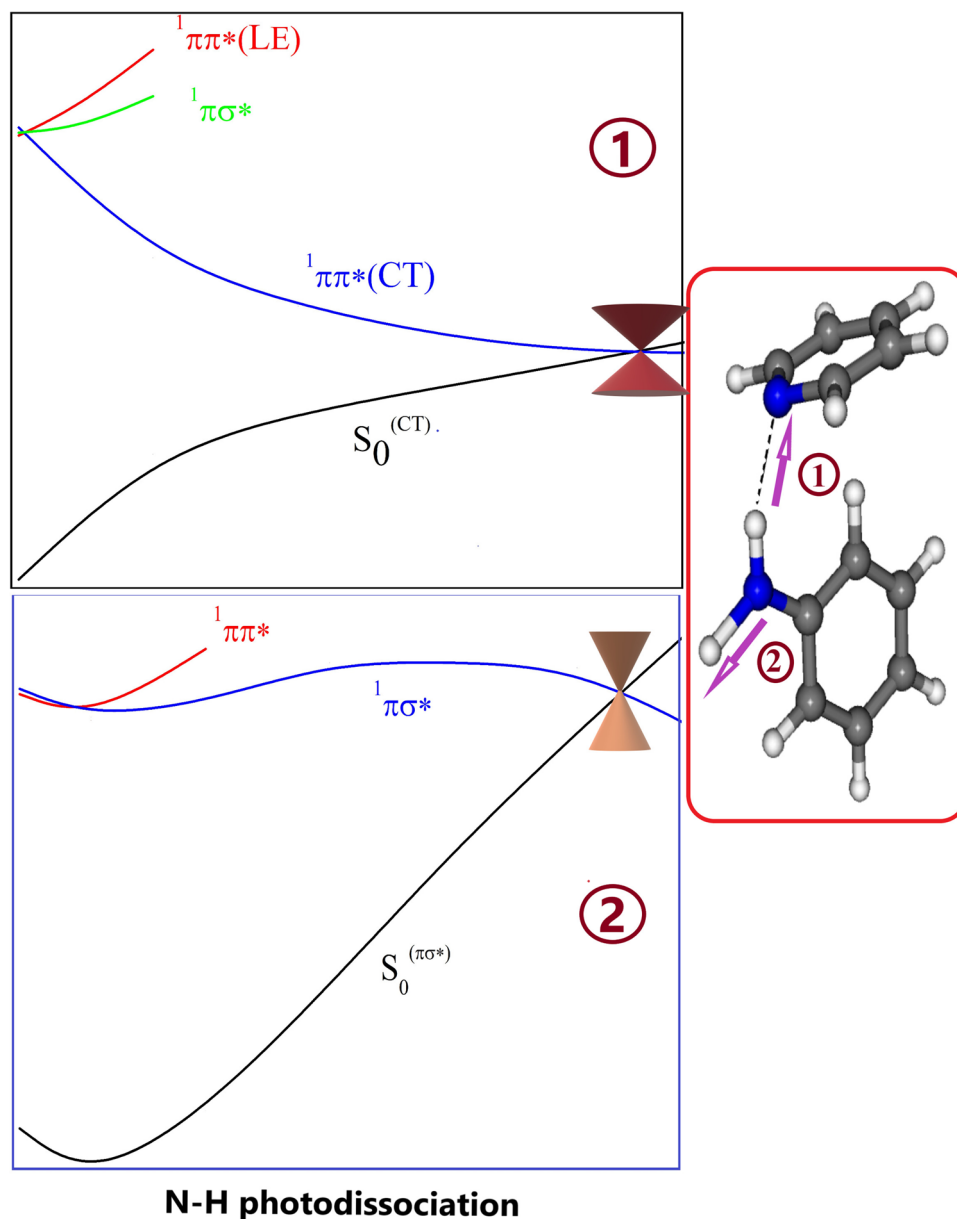
1 Introduction

Aniline ($C_6H_5NH_2$) is an important prototypical aromatic amine for both the photochemistry and photophysics behaviors modeling along the amino moiety in the purine-derived DNA bases guanine and adenine [1, 2]. The dissociative $\pi\sigma^*$ state has been suggested to provide a nonradiative relaxation pathway along its NH_2 coordinates via $\pi\sigma^*/S_0$ conical intersection, leading either to N–H bond dissociation or to the species in the ground state [3].

The photochemistry of isolated aniline has been extensively studied both experimentally [1, 4–17] and theoretically [1, 7, 14–23]. These studies focused mainly on the role of $^1\pi\sigma^*$ channel in the excited state dynamics. Two $^1\pi\sigma^*$ mixed electronic configurations are deduced: Rydberg ($^1\pi3s$) and valence antibonding character ($^1\pi\sigma^*$) states. It has been suggested that in the Franck–Condon (FC) region, the mixed $^1\pi3s/\pi\sigma^*$ state has a significant Rydberg character and changes into a dissociative valence character at longer N–H bond stretching [4, 8, 18]. Whereas, in the case of phenol,

the $^1\pi3s$ and $^1\pi\sigma^*$ components are nearly degenerate in the vertical Franck–Condon region, and the entire potential energy surface will be almost totally dissociative [24, 25].

Works by Ashfold and co-workers [1] and Stavros and co-workers [7] concluded that the non-adiabatic coupling that occurs in the Franck–Condon region is responsible for the transfer of the initially populated $S_1(^1\pi\pi^*)$ state to the $S_2(^1\pi\sigma^*)$ state, leading to the N–H bond fission and the anilino C_6H_5NH radical formation. This photoreaction is energetically accessible for $\lambda = 269.5$ nm.

In addition, the aniline dimer and trimer structures in the ground and lowest electronically excited states have been previously studied [26–28]. These structures are stabilized by hydrogen bonds between the hydrogen of the amino group on one part and the nitrogen atom or with the π electrons of its benzene ring on the other part. To reveal the solvation effects on the photochemistry of aniline, Poterya et al. have investigated the photodissociation dynamics of N–H bonds in aniline in homoclusters $(PhNH_2)_n$ and mixed clusters with water $PhNH_2\text{-}(H_2O)_n$ [15]. For small homoclusters $(PhNH_2)_{n\leq3}$ and small mixed $PhNH_2\text{-}(H_2O)_{n\leq10}$ clusters that presented free N–H bonds, the formation of fast H fragments is attributed to the dissociation on the $\pi\sigma^*$ surface. While on the surface of large water clusters, $(H_2O)_{430}$, they found experimentally that dissociation via $\pi\sigma^*$ state is quenched [15]. In the same context and more recently, $(PhNH_2)_{n\geq3}$ homocluster dynamics along the repulsive $^1\pi\sigma^*$ state have been detected, while the dimer does not present the N–H dissociative $^1\pi\sigma^*$ channel [29].

Among the photochemical reactions involved in these types of molecular hydrogen bonding interactions, hydrogen atom transfer (HAT) or detachment and proton-coupled electron transfer (PCET) have received a wide number of studies [30–33]. However, these mechanisms are different and can be distinguished by the analysis of frontier molecular orbitals, based on whether a proton and an electron are transferred between the same or different sets of molecular orbitals [32], and the potential energy surface characteristics, in terms of the energetic accessibility of the conical intersection between the lowest electronic states [33].

Pyridine is an important biological solvent and is well known as an electron quencher in photochemical reactions. In this study, we have performed investigations of the photochemistry and photophysics processes involved through the N–H bond photodissociation in aniline and the complexes it forms with pyridine $PhNH_2\text{-}(Py)_n$ ($n = 1, 2$). This system is a model for which the proton donor and acceptor are π electron conjugated system. Therefore, it is convenient to compare the N–H photodissociation in both isolated aniline and clustered with pyridine. Aniline undergoes a fast dissociation of the N–H bond as an isolated molecule, while strong hydrogen bonding affects the photodissociation of the N–H bond upon complexation in the Py clusters. We may

ask whether the photochemical and photophysical processes are operative in these kinds of reactions.

To reveal the molecular details of the photochemical and photophysical processes, potential energy profiles of the excited state PCET reactions from $PhNH_2$ to Py as well as hydrogen atom detachment from the NH_2 group of $PhNH_2$ were determined with ab initio calculations. The reaction paths connect the Franck–Condon region of the lowest populated excited state vertically above the ground state equilibrium geometries to the accessible S_1/S_0 conical intersections. Besides, photophysical processes involved in these photochemical reactions were studied to understand and discuss the competition between the radiationless deactivation processes via S_1/S_0 conical intersections in which the complex relaxes back to the electronic ground state and H-atom ejection.

2 Theoretical methods

All calculations were carried out with the TURBOMOLE program package version 5.8 [34]. Ground state structures of $PhNH_2\text{...}(Py)_{1,2}$ were optimized assuming C_s and C_{2v} point group symmetries (if possible) or without any constraints (C_1) at the second-order Moller–Plesset MP2 level within the resolution of identity (RI) approximation for electron repulsion integrals (RI-MP2) [35]. These geometries were used in further calculations of vertical excitation energies. The correlation consistent polarized valence double-ξ basis set of cc-pVDZ quality augmented with diffuse functions (aug-cc-pVDZ) was used for all atoms. The use of diffuse basis functions is required to correctly describe low-lying Rydberg $\pi\sigma^*$ excited states.

Equilibrium geometries of the complexes in neutral and biradical forms in the lowest excited singlet states were calculated via the second-order approximate coupled cluster (CC2) method employing the resolution of identity (RI) approximation [36, 37] using the aug-cc-pVDZ basis set. For both ground and excited state geometry optimizations, starting geometries were constructed with C_s and C_1 symmetry constraints. Within the C_s point group, the aniline molecule lies in the symmetry plane and the excited-state wavefunctions are transformed according to A′ and A″ irreducible representations. The planar structure confers also a C_{2v} point group and an A_1, A_2, B_1 and B_2 electronic states on the excited state. C_s and C_{2v} symmetries were imposed in geometry optimization in some of these calculations due to the near-degeneracy of the lowest excited $^1\pi\pi^*$ and $^1\pi\sigma^*$ states in the Franck–Condon region. To optimize excited state geometries, the minimum energy structure of the ground state was chosen as the starting point for the lowest excited states. Potential energy (PE) profiles were calculated along the minimum energy path (MEP) for elongation of the

N–H stretching coordinate in the $PhNH_2\cdots(Py)_{1,2}$ complex; for a given value of the N–H coordinate, all remaining coordinates were optimized.

3 Results and discussion

3.1 Vertical excitation and equilibrium geometries

The Cartesian coordinates of the optimized geometries are shown in the ESI of this article.

1. Isolated aniline

Free aniline ($PhNH_2$) was constrained to be planar with C_{2v} and C_s symmetries constraints. Vertical excitation energies with associated transitions and oscillator strengths (f) into the low-lying singlet excited state of isolated aniline at its ground state equilibrium geometry were calculated at RICC2/aug-cc-pVDZ level. These specifications for the lowest singlet excited states are reported in Table 1 and compared with previous calculations and experimental values. The two lowest excited singlet states are $^1\pi\sigma^*$ and $^1\pi\pi^*$ are quasi-degenerate with calculated vertical excitation energy of 4.49 eV and 4.51 eV, respectively. The $^1\pi\sigma^*$ state involves the promotion of an electron from the highest π orbital to the lowest diffuse σ^* which is antibonding with respect to the NH bonds (see Fig. 2). It can be seen that the first bright state is of $^1\pi\pi^*$ character with an oscillator strength (f = 0.037) with the contribution percentage of 75%, both of π and π^* orbitals are delocalized over the entire $PhNH_2$ molecule (Fig. 2). However, the second bright $^1\pi\pi^*$ state with an energy transition of 5.44 eV owns the highest oscillator strength (f = 0.228) and will dominate the absorption intensity from the ground state in comparison to the first bright $^1\pi\pi^*$ state. This result is close to previous work, that excitation to the $2^1\pi\pi^*$ state has become an open channel at 240 nm 8. From Table 1 it can be seen that our computed results are in good agreement with the experimental observations of Rajasekhar et al. [9].

Starting from ground state minimum geometry, the lowest excited state geometries of A′ and A″ representations retaining C_s symmetry were optimized by the use of the RICC2/aug-cc-pVDZ method. The states of aniline considered here are the $^1\pi\pi^*$ and the $^1\pi\sigma^*$ excited states, situated energetically below the vertical excitation by about 0.2 and 0.13 eV, respectively.
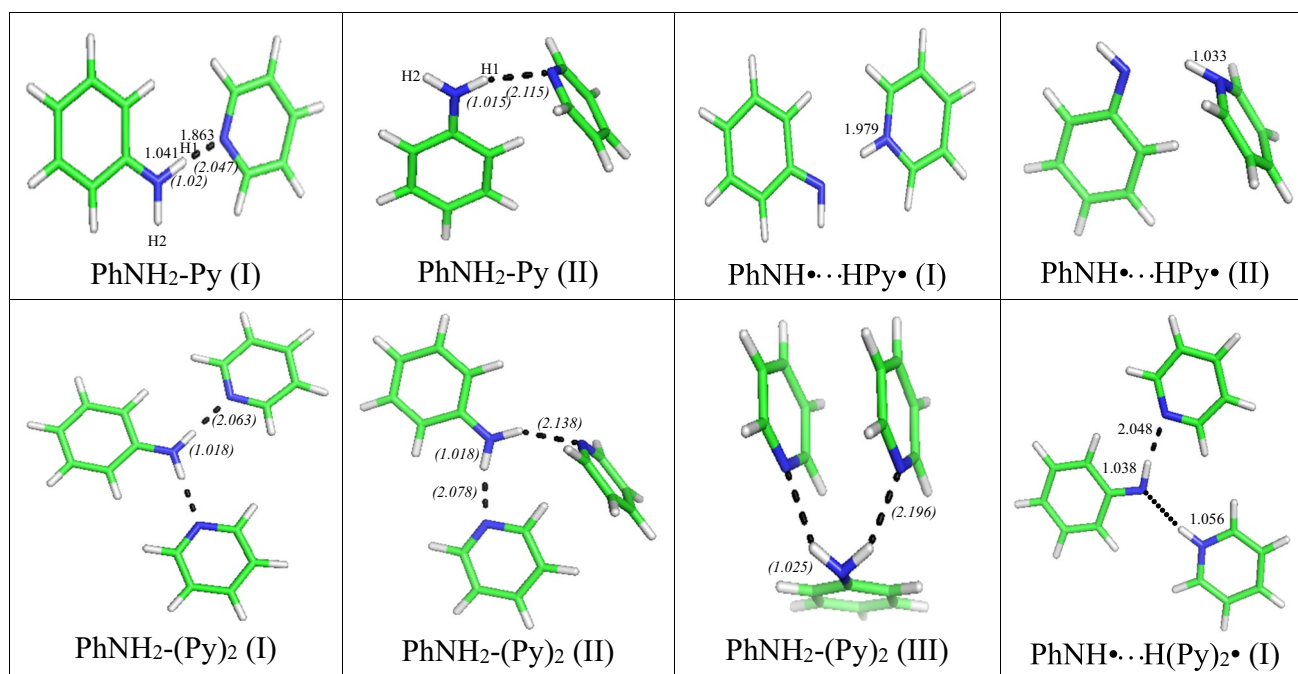
2. $PhNH_2$-Py complex

Two conformers of the $PhNH_2$-Py complex that exhibit an intermolecular hydrogen bond between an N–H of $PhNH_2$ moiety and the N atom of the Py moiety have been considered. These two conformers are presented for the mutual orientation of the $PhNH_2$ molecule vis-a-vis the Py molecule. The first (conformer (I)) displays C_s symmetry, all atoms of the complex $PhNH_2$–Py were constrained to be in the same plane. The second conformer (II) displays also C_s symmetry and forming a T-shaped structure in which the pyridine molecule becomes in the plane perpendicular to the molecular plane of aniline. These two conformers in the ground state have no change in equilibrium geometry and energy when constraints were removed (C_1 symmetry). Both planar and T-shaped conformers exhibit a strong hydrogen bond NH1$\cdots$N between aniline and the nitrogen atom of pyridine, in which aniline is an H atom donor. The second hydrogen atom of the amino group NH_2 denoted H_2 is free hydrogen in both conformers.

Figure 1 shows the ground state (S_0) equilibrium geometries of the $PhNH_2$–Py complex with (C_s) and without symmetry constraints ((I) and (II) conformers), which were optimized at the RI-MP2 level using the aug-cc-pVDZ basis set. The hydrogen bond length is increased by more than 0.07 in favor of the conformer (II) when the $PhNH_2$–Py complex is changed from planar (I) to T-shaped (II). Moreover, the hydrogen bond length between the H_1 and N atoms is 2.047 and 2.115 Å for the hydrogen-bonded (I) and (II) conformers, respectively, and the N–N distances are 3.066 and 3.088 Å, respectively. Additionally, dissimilarly to conformer (II), the hydrogen bond angle in the conformer (I)

Table 1 Vertical excitation energies (eV) and oscillator strengths f of the lowest singlet excited states of isolated aniline at the ground state minimum under C_{2v} and C_s symmetries, computed at the RICC2 level with the aug-cc-pVDZ basis set and compared with values from previous ab initio calculations and experimental values

C_{2v}	C_s	RICC2 (This work)			CAS2/XMC-QDPT2 [21]	SAC-CI [18]	MS-CASPT2 [19]	CR-EOM-CCSD(T) [20]	Exp [9]
		State	E (eV)	f	E (eV)	E (eV)	E (eV)	E (eV)	E (eV)
B_2	A″	$1\,^1\pi\sigma^*$ (77%)	4.49	0.005	4.74	4.53	4.85	4.69	–
B_1	A′	$1\,^1\pi\pi^*$ (75%)	4.51	0.037	4.22	4.20	4.33	4.21	4.41
A_1	A′	$2\,^1\pi\pi^*$ (64%)	5.44	0.228	5.25	5.34	5.54	5.42	5.42
B_2	A″	$2\,^1\pi\sigma^*$ (76%)	5.82	0.018	6.25	6.39	6.28	–	5.78

Fig. 1 Ground and excited states optimized structures of PhNH$_2$-Py and PhNH$_2$-(Py)$_2$ and their corresponding electron/proton transferred complexes (biradicals). Distances are given in Å
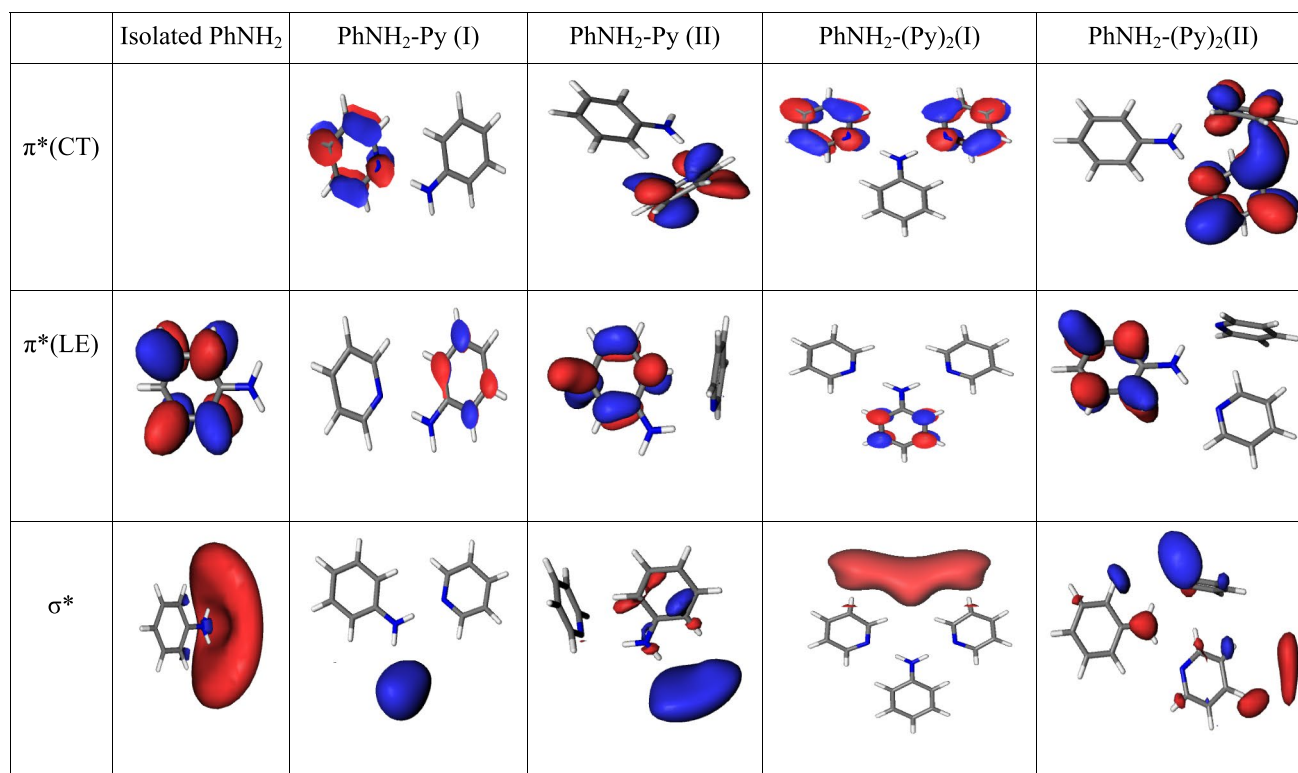
is very close to 180°. Although all these values comparison are in favor of more stability of the conformer (I), the RICC2 level of theory predicts the lowest energy to be the conformer (II) with a difference in stability of about 0.1 eV. This can be explained by the existence of CH···π hydrogen bond which certainly contributes to the stabilization of the conformer (II). This interaction involves an aromatic CH donor (aniline) and an aromatic π system as acceptor (pyridine). Therefore, conformer (II) of PhNH$_2$-Py is stabilized by two hydrogen bonds NH1···N and CH···π. Several studies have been interested in the aromatic CH···π hydrogen bonds (T-shaped interactions) [38–40]. It has been suggested that aromatic CH···π hydrogen bonds play an important role in the stability of 3D structures of biological macromolecules (proteins, DNA, …). The major source of attraction in the CH···π interaction is the dispersion interaction and the

electrostatic contribution is small, while the electrostatic interaction is mainly responsible for the attraction in the conventional H-bonds [41].

Vertical excitation energies with corresponding transitions and oscillator strengths of the conformers (I) and (II) of the PhNH$_2$···Py complex were calculated. Table 2 shows these parameters for the lowest five singlet excited states in both A′ and A″ symmetries. At the RICC2/aug-cc-pVDZ level of theory, the calculation shows a quasi-degenerate lowest $^1\pi\pi^*$ and $^1\pi\sigma^*$ states for both conformers (I) and (II), which exhibits a vertical excitation energy difference about 0.02 and 0.03 eV, respectively. The lowest ^{1}A″ state is of $^1\pi\sigma^*$ character and $^1\pi\pi^*$ nature for conformer (I) and conformer (II), respectively. For conformer (I) in Fig. 2, the $^1\pi\sigma^*$ excited state arises from the excitation from the 7a″(π) orbital to the diffuse σ* orbital (29a′), while

Table 2 Vertical excitation energies (eV) and oscillator strengths f of the lowest five singlet excited states for conformers (I) and (II) of PhNH$_2$-Py complex at the ground state minimum under C$_s$ symmetry, computed at the RICC2 level with the aug-cc-pVDZ basis set

PhNH$_2$-Py (I)			PhNH$_2$-Py (II)		
State	E (eV)	f	State	E (eV)	f
1A″ $^1\pi\sigma^*$ (46%)	4.36	0.004	1A′ $^1\pi\pi^*$(LE) (24%)	4.40	0.037
2A′ $^1\pi\pi^*$(LE) (60%)	4.38	0.040	2A″ $^1\pi\sigma^*$ (35%)	4.43	0.003
3A″ $^1\pi\sigma^*$ (31%)	4.75	0.000	3A″ $^1\pi\pi^*$(CT) (23%)	4.48	0.001
4A′ $^1\pi\pi^*$(CT) (82%)	4.78	0.014	4A″ $^1\pi\sigma^*$ (33%)	4.83	0.000
5A″ $^1\pi\sigma^*$ (29%)	4.97	0.000	5A′ $^1\pi\pi^*$CT (61%)	4.96	0.028

	Isolated PhNH$_2$	PhNH$_2$-Py (I)	PhNH$_2$-Py (II)	PhNH$_2$-(Py)$_2$(I)	PhNH$_2$-(Py)$_2$(II)
π*(CT)					
π*(LE)					
σ*					

Fig. 2 Molecular virtual orbitals involved in vertical electronic transitions in isolated aniline and PhNH$_2$-(Py)$_n$ ($n = 1,2$) complexes

excitation from the 7a"(π) orbital to the 11a"(π*) orbital which are entirely localized on aniline, gives rise to the lowest locally excited $^1\pi\pi$*(LE) state. For conformer (II) in Fig. 2, the LE and the $^1\pi\sigma$* excited states are attributed both to excitation of the 10a"(π) orbital to the 16a"(π*) orbital and the diffuse σ* orbital (25a'), respectively. The diffuse orbital is extremely sensitive to the NH bond lengths and is localized mainly on the amino group of aniline upon vertical excitation. As a result, when one of the NH bond lengths is slightly extended, this orbital collapses to the 1 s orbital of the departing H-atom as is well demonstrated for acidic aromatic systems [3]. These two states are followed by $^1\pi\pi$*(CT), where π is located on PhNH$_2$ and π* is located on Py.

The vertical energy difference between the lowest $^1\pi\pi$*(LE) excited state and the lowest CT state is higher for the conformer (I) by about 0.32 eV than the corresponding value for the conformer (II). Indeed, when passing from the conformer (I) to the conformer (II), the excitation energies of the $^1\pi\sigma$* and $^1\pi\pi$*(LE) are slightly shifted to greater values by 0.02 and 0.07 eV, respectively. Whereas the position of the lowest $^1\pi\pi$*(CT) state is shifted to significantly lower energy by 0.3 eV. As a result, the energy gap between LE and CT states was reduced to 0.08 eV in the case of the T-shaped conformer. This is mainly the result of the

contributions of two acidic sites NH1···N and CH···π on the stability of the conformer (II).

Compared to the isolated aniline, the vertical excitation energy of the $^1\pi\sigma$* and $^1\pi\pi$* states in conformer (I) are both redshifted by 0.13 eV, while in conformer (II) these states are redshifted by 0.06 and 0.11 eV, respectively.

3. PhNH$_2$-(Py)$_2$ complex

The structures of optimized PhNH$_2$-(Py)$_2$ conformers (I), (II), and (III) are shown in Fig. 1. It should be noted that the structures of these complexes are the most suitable to facilitate the formation of the conical intersection. Conformer (I) with its planar structure (all atoms in the same plane) may be regarded as belonging to both C$_{2v}$ and C$_s$ symmetries and involves pyridine molecules binding to each H atom of the amino group of aniline similarly to PhNH$_2$-Py but with stronger interactions, in which two hydrogen atoms of the amino group interact with two Py molecules. The bond lengths and energies of C$_s$ and C$_{2v}$ optimized geometries are very similar.

T-shaped conformer (II) presents a combined planar and T-shaped structure, in which one Py is in the same plane with PhNH2 and interact through NH···N hydrogen bonding, the second Py forms a CH···π interaction on one side of

the Py ring in addition to the NH···N interaction. This latest conformer is calculated to be more stable by about 0.15 eV.

The third conformer (III) is stabilized by two H bonds like conformer (I) and by a π-π interaction between the pyridine molecules, which are parallel and located face-to-face forming a sandwich separated by about 3.5 Å. (see Fig. 1). The calculation indicates that the formation of the sandwich dimer of pyridine in the complex causes an energy redshift by about 0.48 eV compared with the conformer (I) due to π-π stacking interaction between the indicated molecules. This structure of pyridine dimer in this complex is analog to other molecular systems like benzene dimer, benzene-phenol, benzene-toluene [42, 43].

Vertical excitation energies with corresponding transitions and oscillator strengths for all considered conformers of the $PhNH_2$–$(Py)_2$ complex calculated using RICC2/aug-cc-pVDZ method are presented in Table 3. As it is shown, for the planar conformer (I), the two lowest excited states are of the dark $^1\pi\sigma^*$ and bright $^1\pi\pi^*$(LE) features and are quasi-degenerate at 4.2 eV, and the oscillator strengths of these states are 0.002 and 0.04. The next higher states are two $^1\pi\pi^*$(CT) at 4.4 eV. The molecular orbitals involved in these two electronic excitations are presented in Fig. 2. For T-shaped conformer (II), The excitation spectrum consists of a low-lying dark $^1\pi\pi^*$(CT) at 4.19 eV. The transition into this state from the ground electronic state is unlikely, as indicated by the small oscillator strength (f = 0.000). While the first bright $^1\pi\pi^*$(LE) is at 4.31 eV with oscillator strength 0.035 and is exactly degenerate with the $^1\pi\sigma^*$ state. In conformer (III), the $^1\pi\pi^*$(LE) state disappears in the five first lowest excited states. However, the S_1 and S_2 states are of $^1\pi\pi^*$(CT) character and are bright in absorption with excitation energies of 4.45 and 4.56 eV and oscillator strengths of 0.028 and 0.013, respectively. The two lowest $^1\pi\sigma^*$ excited states lie higher in energy in the vertical excitation spectrum (4.69 and 4.79 eV).

3.2 Photophysical and photochemical processes through N–H bond photodissociation

The N–H bond photodissociation channel was recognized as one of the primary radiationless deactivation mechanisms as well as H-atom elimination in a variety of systems in the gas phase. Since, when complexed with pyridine, there are two such bonds in $PhNH_2$, free and hydrogen bonded, both types were considered in each of aniline-pyridine complexes to investigate the photophysical processes and photochemical reactions. The $^1\pi\pi^*$ and $^1\pi\sigma^*$ excited electronic states have been identified to play an important role in photophysical processes for these types of complexes: DNA/RNA nucleobases, aromatic amino acids and their corresponding chromophore subunits [3, 11, 24, 44], malonaldehyde, o-hydroxybenzaldehyde, salicylic acid and 7-hydroxy-1-indanone [45, 46], indole-water clusters [47], and phenol-water and phenol-ammonia clusters [48]. To reveal the existence of conical intersections and the possibility of an internal conversion between the excited $^1\pi\pi^*$ and $^1\pi\sigma^*$ states and the ground state S_0, it is required to scan the PES of these states, to estimate the energy barrier between the Franck–Condon region and CI.

3.2.1 Proton Coupled Electron Transfer PCET

1. $PhNH_2$–Py

The potential energies of the lowest excited singlet and ground states along the N-H1 bond length of aniline in the conformers (I) and (II) of the $PhNH_2$–Py complex are explored in this section. Here, for a fixed value of the N–H1 coordinate, all remaining coordinates were optimized. Figure 3a and b depict the potential energy profiles of the S_0 and singlet states. The potential energy functions along the reaction coordinate were constructed by stretching the N-H1 bond by steps of 0.1 Å or 0.2 Å. Along the reaction path, the geometry of the lowest $^1\pi\pi^*$(CT) singlet state was

Table 3 Vertical excitation energies (eV) and oscillator strengths f of the lowest five singlet excited states for conformers (I), (II) and (III) of $PhNH_2$-$(Py)_2$ complex at the ground state minimum under C_{2v}, C_s and C_1 symmetry, respectively. computed at the RICC2 level with the aug-cc-pVDZ basis set

$PhNH_2$-$(Py)_2$ (I)					$PhNH_2$-$(Py)_2$ (II)				$PhNH_2$-$(Py)_2$ (III)		
Sym		State	E (eV)	f	Sym	State	E (eV)	f	State	E (eV)	f
C_s	C_{2v}			C_s							
A″	B_2	1 $^1\pi\sigma^*$ (39%)	4.22	0.002	A″	1 $^1\pi\pi^*$(CT) (57%)	4.19	0.000	1 $^1\pi\pi^*$(CT)(18%)	4.45	0.028
A′	B_1	2 $^1\pi\pi^*$(LE) (48%)	4.23	0.040	A′	2 $^1\pi\pi^*$(LE) (32%)	4.31	0.035	2 $^1\pi\pi^*$(CT)(38%)	4.56	0.013
A′	A_1	3 $^1\pi\pi^*$(CT) (74%)	4.40	0.012	A″	3 $^1\pi\sigma^*$ (32%)	4.31	0.001	3 $^1\pi\sigma^*$ (24%)	4.69	0.007
A′	B_1	4 $^1\pi\pi^*$(CT) (87%)	4.43	0.011	A′	4 $^1\pi\pi^*$(CT) (79%)	4.46	0.073	4 $^1\pi\sigma^*$ (9%)	4.79	0.013
A″	B_2	5 $^1\pi\sigma^*$ (36%)	4.51	0.000	A′	5 $^1\pi\pi^*$(CT) (63%)	4.65	0.044	5 $^1\pi\pi^*$(CT)(26%)	4.96	0.007
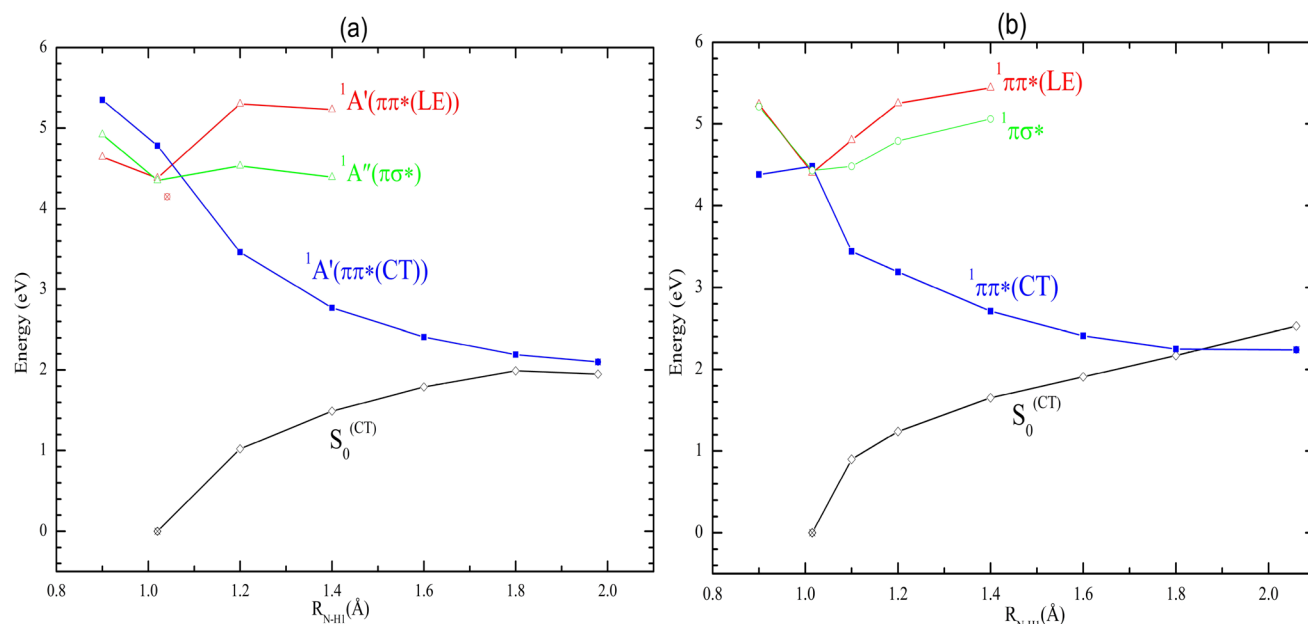
Fig. 3 Potential energy profiles along the N-H1 stretching coordinate of the PhNH$_2$–Py complex, **a** planar structure (conformer (I)) and **b** T-shaped (conformer (II)), calculated with the RICC2 method. For $R_{N-H1} = 1.02$ Å, at the optimized energy of the electronic ground state S_0(open diamond), the lowest singlet $^1\pi\sigma^*$ (open green circle), $^1\pi\pi^*$(LE) (open red triangle) and $^1\pi\pi^*$(CT) (blue filled square) excited states were calculated at this point. For $R_{N-H1} > 1.02$ Å, S_0, $^1\pi\sigma^*$ and $^1\pi\pi^*$(LE) were calculated at optimized geometries of the $^1\pi\pi^*$(CT) state. The (open times) symbol represents the minimum energy of neutral and biradical PhH•···HPy• complexes. The RICC2 ground state energy computed at the corresponding RI-MP2 optimized geometry is used as the reference energy

optimized, whereas the energies of the electronic ground (S_0) and excited singlet ($^1\pi\pi^*$(LE) and $^1\pi\sigma^*$) states were calculated along the reaction path optimized in the $^1\pi\pi^*$(CT) state. The $^1\pi\pi^*$(LE) and $^1\pi\sigma^*$ states are energetically too high to play a significant role in the photophysics of the two conformers near the Franck–Condon region.
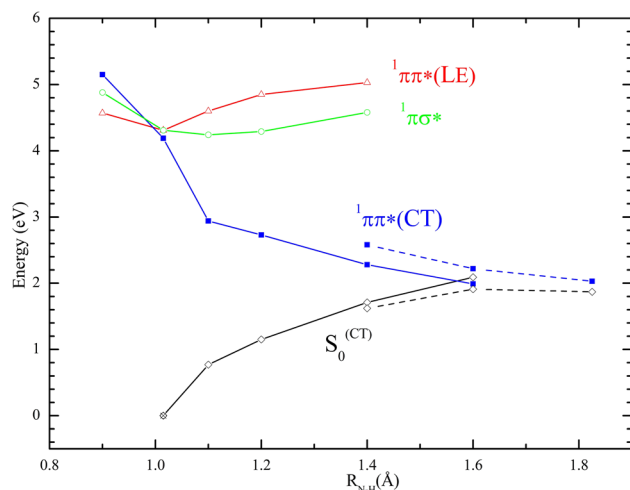
As the N-H1 coordinate is elongated, the potential energy of the $\pi\pi^*$(LE) state increases and the energy of the $^1\pi\pi^*$(CT) state in which an electron from the π orbital of PhNH$_2$ is promoted to the π^* orbital of Py decreases rapidly. Vertical excitation energies indicate that the CT state is the fourth and third electronic state for planar and T-shaped conformers, respectively. This CT appears upon a slight elongation of the distance between the donor N of the amino group and the acceptor N atom of Py involved in the hydrogen bond. This induces a PCET reaction, which can occur via stepwise mechanisms, with the electron being transferred first, followed by the proton transfer.

For R_{N-H1} smaller than 1.6 Å, optimization of the structures of conformers (I) and (II) without symmetry constraints leads to the nearly T-shaped structure. Furthermore, when the R_{N-H1} distance is further stretched, the energy of the CT state decreases, the charge separation exerts a strong force on the proton to follow the electron. The proton then

crosses the hydrogen bond transition state and attaches to the N atom of pyridine leading to a strong energetic stabilization radical pair PhH•···HPy•. The photophysics of conformer (I) in Cs symmetry (A′ representation) differ from the second (II) at a larger reaction coordinate (see Fig. 3a). However, in its final structure (biradical), the excited $^1\pi\pi^*$(CT) sate of conformer (I) (planar structure) has an energy about 0.15 eV above the ground state which makes the $^1\pi\pi^*$(CT)/S_0 crossing not detected, it may occur at a larger distance. Along this reaction, we also found a $^1\pi\pi^*$(LE)/$^1\pi\pi^*$(CT) conical intersection near the Franck–Condon region with a small barrier (0.16 eV). Whereas for conformer (II) (T-shaped), the proton transfer stabilizes the $^1\pi\pi^*$(CT) sate and the S_0 energy computed at the $^1\pi\pi^*$(CT) geometries is destabilized. Consequently, the barrierless energy curve of the $^1\pi\pi^*$(CT) state crosses the S_0 energy profile at $R_{NH1} = 1.855$ Å with an energy of 2.25 eV above the S_0 minimum (see Fig. 3b). Since both energy profiles are calculated at the same geometries, the crossing of these curves is a true energy crossing, and it represents a conical intersection. These results show that after crossing the conical intersection between the ground and excited states, the photoreaction can lead to the formation of a stabilized biradical or to internal conversion to the ground state of the complex.

2. PhNH$_2$–(Py)$_2$

The photophysics of the electronically excited and ground states of the PhNH$_2$–(Py)$_2$ complex without any symmetry constraint is linked to the N–H bond photodissociation. It entails investigating the potential energies of the lowest excited singlet and ground states along the N–H reaction coordinate and decaying at a region of excited and ground states degeneracy (near the expected S$_1$/S$_0$ conical intersection). The potential energy profiles of the S$_0$, $^1\pi\pi^*$(LE) and $^1\pi\pi^*$(CT) states leading to the most relevant feature of the deactivation mechanism are summarized in Fig. 4. along the reaction path, the geometry of the lowest $^1\pi\pi^*$(CT) singlet state was optimized, whereas the energies of the electronic ground (S$_0$) and excited singlet ($^1\pi\pi^*$(LE) and $^1\pi\sigma^*$) states were calculated along the reaction path optimized in the $^1\pi\pi^*$(CT) state. Optimization of the planar complex (conformer (I)) without symmetry constraints leads to the T-shaped structure (conformer (II)) for R$_{N-H}$ less than 1.4 Å. As a result, for the planar conformer, we reduced the PE profiles only for R$_{N-H} \geq 1.4$ Å. As previously stated, the $^1\pi\pi^*$(LE) and $^1\pi\sigma^*$ states are higher in energy and do not play a role in photophysics. PE profiles of the T-shaped conformer, as shown in Fig. 4, need not require any crossing between the $^1\pi\pi^*$(LE) and $^1\pi\pi^*$(CT) states. The decay of the T-shaped structure, on the other hand, is attributed to direct

relaxation from the first repulsive $^1\pi\pi^*$(CT) state to the S$_0$ state, giving rise to a conical intersection at R$_{NH}$ = 1.57 Å with an energy of 2.03 eV above the S$_0$ minimum. This CI represents a pathway for either ultrafast internal conversation to the ground state or biradical formation. Whereas the planar structure appears only between R$_{NH}$ = 1.2 Å and 1.4 Å. The potential energy of its lowest $^1\pi\pi^*$(CT), where the proton follows the electron and attaches to the N atom of pyridine, leads to the neutralization of ion pair and the formation of the stable PhH•···H(Py)$_2$• biradical complex at R$_{NH}$ = 1.825 Å, decreases significantly. This biradical, which is produced through unidirectional PCET has an energy of roughly 0.19 eV higher than the ground state.

3.2.2 H-atom detachment from aniline

1. Isolated PhNH$_2$

Calculated Potential energy (PE) profiles for the H-atom detachment reaction from the amino group NH$_2$ of free aniline are shown in Fig. 5. The energies of the ground S$_0$ state were calculated at geometries which were optimized in the $^1\pi\sigma^*$ state for fixed N–H bonds. Also, geometries of the lowest $^1\pi\pi^*$ excited state were optimized along the reaction coordinate. As it is shown in this figure the two lowest singlet excited state $^1\pi\pi^*$ are bound and parallel to the PE function of the electronic S$_0$ state, while the PE profile of the
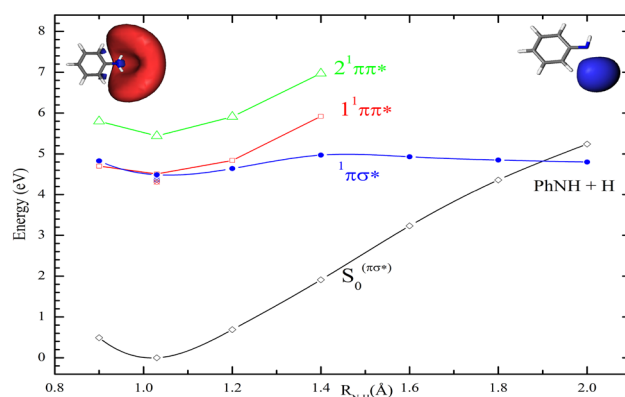

Fig. 4 Potential energy profiles along the N–H stretching coordinate of the PhNH$_2$–(Py)$_2$ complex, planar conformer (I) (dashed line) and T-shaped conformer (II) (solid line), calculated with the RICC2 method. For R$_{NH}$ = 1.015 Å, at the optimized energy of the electronic ground state S$_0$(open diamond), the lowest singlet $^1\pi\sigma^*$ (open cicle), $^1\pi\pi^*$(LE) (open triangle) and $^1\pi\pi^*$(CT) (filled black square) excited states were calculated at this point. For R$_{NH}$ > 1.015 Å, S$_0$, $^1\pi\sigma^*$ and $^1\pi\pi^*$(LE) were calculated at optimized geometries of the $^1\pi\pi^*$(CT) state. The (open times) symbol represents the minimum energy of biradical PhH•···H(Py)$_2$• complex. The RICC2 ground state energy computed at the corresponding RI-MP2 optimized geometry is used as the reference energy

Fig. 5 Potential energy curves of isolated PhNH$_2$ along the N–H bond stretch coordinate at the planar geometry, obtained at the RICC2/aug-cc-pVDZ level. For R$_{NH}$ = 1.01 Å, at the optimized energy of the electronic ground state S$_0$(open diamond), the lowest singlet $^1\pi\sigma^*$ (filled black circle), 1$^1\pi\pi^*$ (open square) and 2$^1\pi\pi^*$ (open triangle) excited states were calculated at this point. For R$_{N-H}$ < 1.01 Å and R$_{N-H}$ > 1.01 Å, S$_0$ and 1$^1\pi\pi^*$ and 2$^1\pi\pi^*$were calculated at optimized geometries of the $^1\pi\sigma^*$ state. The (open times) symbol represents the minimum energy of the neutral complex. The RICC2 ground state energy computed at the corresponding RIMP2 optimized geometry is used as the reference energy. The top left and top right insets show σ^* natural orbital of the $^1\pi\sigma^*$ state obtained at its equilibrium geometry and at a stretched N–H bond length (R$_{N-H}$ = 2.0 Å) of the amino group, respectively

lowest excited state $^1\pi\sigma^*$ is dissociative with an exit barrier to N–H dissociation of about 0.5 eV with the maximum is located near 1.4 Å. This result provides the possibility of a relatively longer excited state lifetime for the hydrogen detachment mechanism. This barrier separates the Rydberg (diffuse) part of the PE function and the valence (repulsive) part, in which the σ^* orbital collapses to the 1 s orbital of the hydrogen atom. In the same figure (Fig. 5), molecular orbitals involved in the lowest excited states of isolated aniline at the starting of the reaction and near the conical intersection, are shown.

The population of the dark $^1\pi\sigma^*$ state from the bright $^1\pi\pi^*$ state occurs easily because the optimized $^1\pi\sigma^*$ and $^1\pi\pi^*$ states are quasi-degenerate in the Franck–Condon region, with an energy difference about 0.02 eV. In this region, the $^1\pi\sigma^*$ state has shallow local minima. When the N–H bond was stretched to 1.9 Å, a $^1\pi\sigma^*/S_0$ energy crossing was found at an energy about 4.82 eV above the ground state minimum and 0.33 eV above to the starting point (Franck–Condon region). Furthermore, because the appropriate PE profiles were computed at the same geometry optimization, this $^1\pi\sigma^*/S_0$ conical intersection is real. As a result, a $^1\pi\sigma^*/S_0$ conical intersection is highly probable; therefore, detachment of hydrogen from isolated aniline may cause competition between nonradiative decay to the ground state and H atom elimination. This result is qualitatively supported by previous studies [18].

2. $PhNH_2$–Py

It is required to determine the PE profiles of the two lowest $^1\pi\pi^*$ and $^1\pi\sigma^*$ states along the reaction coordinate, to show the presence of a conical intersection, the possibility of an internal conversion between the excited state S_1 and the ground state and to estimate the energy barrier between the Franck–Condon region and CI. The electron/proton-transfer detachment over the N–H2 bond length of aniline in the conformers (I) and (II) of the PhOH–Py complex was followed using RICC2/aug-cc-pVDZ computations. Figure 6a and b show potential energy (PE) profiles calculated along the minimum energy path (MEP) for elongation of the N–H2 stretching coordinate in the conformers (I) and (II) in C_1 symmetry; all remaining coordinates were optimized for the lowest $^1\pi\sigma^*$ excited state for a given value of the N–H2 coordinate. Along the N–H2 reaction coordinate, the energy of the ground state and $^1\pi\pi^*$ state were calculated on the basis of the S_1 optimized geometry.

As one can see from Fig. 6, the reaction coordinates connect the Franck–Condon region and the $^1\pi\sigma^*/S_0$ CI geometry. It appears that hydrogen atom detachment takes place on the $^1\pi\sigma^*$ surface and requires a crossing of a barrier of 0.5 eV and 0.56 eV with respect to the Franck–Condon geometries of conformers (I) and (II), respectively. The energy barrier is associated with the Rydberg (diffuse) to valence transformation of the σ^* orbital [3]. The diffuse
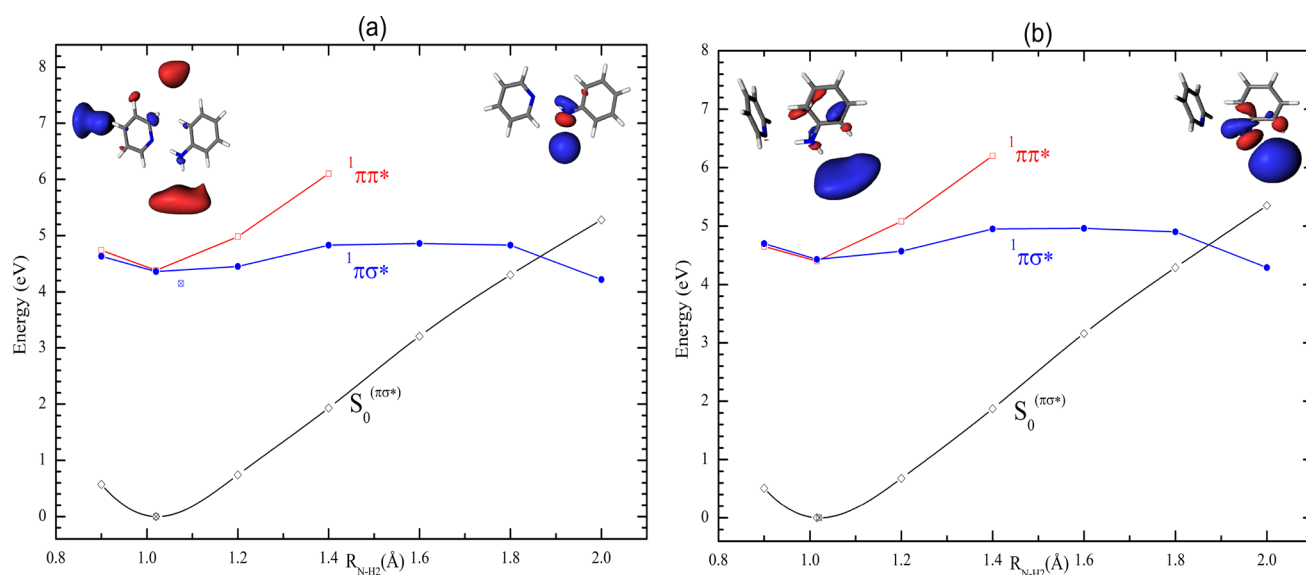
Fig. 6 Potential energy profiles along the N-H2 stretching coordinate of the PhNH$_2$–Py complex, **a** planar structure (conformer (I)) and **b** T-shaped (conformer (II)), calculated with the RICC2 method. For $R_{N-H2} = 1.02$ Å, at the optimized energy of the electronic ground state S_0(open square), the lowest singlet $^1\pi\sigma^*$ (filled black circle) and $^1\pi\pi^*$ (open square) excited states were calculated at this point. For $R_{N-H2} < 1.02$ Å and $R_{N-H2} > 1.02$ Å, S_0 and $^1\pi\pi^*$ were calculated at

optimized geometries of the $^1\pi\sigma^*$ state. The ($\otimes$) symbol represents the minimum energy of the neutral complex. The RICC2 ground state energy computed at the corresponding RIMP2 optimized geometry is used as the reference energy. The top left and top right insets show σ^* natural orbital of the $^1\pi\sigma^*$ state obtained at its equilibrium geometry and at a stretched N–H bond length ($R_{N-H2} = 2.0$ Å) of the amino group, respectively

orbital at the Franck–Condon geometry (equilibrium geometry), and the valence orbital towards the 1 s valence orbital of the hydrogen atom detachment (H2 atom) are presented in Fig. 6. In both conformers, the PES profile of the $^1\pi\sigma^*$ state along the N–H2 coordinate and after exiting the barrier is dissociative. For planar conformer (I), the stretching of the N–H2 bond of the amino group leads to a $^1\pi\sigma^*/S_0$ crossing at an N-H2 bond length of 1.87 Å and energy of 4.66 eV above the S_0 minimum. While for T-shaped conformer (II), The conical intersection occurs at an N–H2 bond length of 1.87 Å and at an energy of 4.68 eV above its S_0 minimum. Following the $^1\pi\sigma^*/S_0$ crossing, there may be a competition between internal conversion to the ground state and H-atom ejection upon evolution on the dissociative part of the $^1\pi\sigma^*$ state. In the former mechanism, the electronic energy is converted primarily into the N-H2 stretching vibration. In the latter mechanism, the electronic energy is converted into kinetic energy of the ejected hydrogen atom. As a result, the complex may promote photochemical H2 generation.

3.3 Discussion

Photochemical reactions and photophysical processes induced by the formation of hydrogen bonds have already been studied for a family of heterocyclic compounds that possess both a proton donor (OH, NH, or NH_2 group) and the nitrogen (N) atom of pyridine as an acceptor [25, 49–59]. The common feature of all results is based on the arguments of Mataga and coworkers [55]. Fluorescence quenching was commonly generated by intermolecular hydrogen-bonding interaction, especially it consists of a generic model of fluorescence quenching when two conjugate π-electronic systems were interacted. For hydrogen-bonded complex in the excited state, a slight proton shift from donor toward acceptor appears to induce CT followed by a large-scale proton transfer. After the CT/S_0 conical crossing, an ultrafast radiationless transition to the vibrational ground state of the hydrogen bond occurs. The possibility of an excited state proton transfer from $PhNH_2$ to the pyridine molecule has been investigated. To reach another minimum for the $PhNH_2$–Py clusters on the $^1\pi\pi^*$(CT) surface, the N–H bond has thus cleaved. This minimum was found for all the studied clusters, and it consists of PhNH•···HPy• radicals. The CT state of the radical complex and the $^1\pi\pi^*$(CT)/S_0 conical intersection lie below the vertical excitation (Franck–Condon region) of the neutral form by about 2.7 and 2.1 eV, respectively. Adding one more Py molecule lowers the energy difference by more than 0.5 eV for the former one and slightly increases (0.07 eV) the $^1\pi\pi^*$(CT/S_0) conical intersection. For all the studied clusters, the energetic barrier calculated for this PCET process is too small or barrierless. Here, when both O − H bonds of NH_2 groups are hydrogen

bonded to multiple Py molecules, the H-atom elimination channel remains suppressed.

For the H-atom detachment, the $^1\pi\sigma^*/S_0$ conical intersection lies about 0.3 eV above the Franck–Condon excitation for both isolated aniline and monomer complex. Moreover, for the T-shaped $PhNH_2$-Py conformer this intersection is located at 2.43 eV above the $^1\pi\pi^*$(CT)/S_0 one. This result is in favor of the PCET reaction than the H-atom detachment in the same conformer exhibiting both N–H···H hydrogen bonding and free N–H bond.

In this respect, nonradiative decay for the PCET reaction could be described as ultrafast and is assigned to barrierless $\pi\pi^*$(CT) deactivation, whereas relatively slower decay for the H-atom detachment reaction is assigned to $^1\pi\sigma^*$ deactivation after overcoming an energy barrier about 0.5 eV.

4 Conclusion

In this contribution, a systematic study of the nonradiative decay processes and photochemical pathways has been explored through the RICC2 level of theory. The PE profiles of the coupled electron-proton transfer photoreactions in the hydrogen-bonded complexes of aniline with pyridine have been computed along reaction coordinates. Two main excited-state reaction mechanisms have been identified in $PhNH_2$-(Py)$_n$ ($n = 1,2$) complexes. The first is the excited state proton-coupled electron transfer (PCET) from aniline molecule to pyridine through hydrogen bonding. The calculated PE profiles are governed mainly by a repulsive $^1\pi\pi^*$(CT) state and reveal the existence of a barrierless path for PCET, leading to a low-lying $^1\pi\pi^*$(CT)/S_0 conical intersections along hydrogen-bonded reaction paths from $PhNH_2$ to Py which can promote ultrafast excited state deactivation or stabilization to a biradical complex.

Another photophysical reaction mechanism identified is hydrogen atom detachment in complexes exhibiting free hydrogen in the amino group of aniline. The energy profiles of this reaction are the same for the two conformers. The N–H dissociation occurs via the dissociative $^1\pi\sigma^*$ state, where a conical intersection with the S_0 state can be reached after overcoming an energy barrier leading both to nonradiative relaxation to the S_0 minimum or generation of H atom radicals. These radicals may subsequently react with each other to produce H_2 molecules.

Declarations

References

1. King, G. A., Oliver, T. A. A., & Ashfold, M. N. R. (2010). Dynamical insights into $^1\pi\sigma^*$ state mediated photodissociation of aniline. *Journal of Chemical Physics, 132*(21), 214307. https://doi.org/10.1063/1.3427544

2. Schultz, T., Samoylova, E., Radloff, W., Hertel, I. V., Sobolewski, A. L., & Domcke, W. (2004). Efficient deactivation of a model base pair via excited-state hydrogen transfer. *Science, 306*(5702), 1765–1768. https://doi.org/10.1126/science.1104038

3. Sobolewski, A. L., Domcke, W., Dedonder-Lardeux, C., & Jouvet, C. (2002). Excited-state hydrogen detachment and hydrogen transfer driven by repulsive $^1\pi\sigma^*$ states: A new paradigm for nonradiative decay in aromatic biomolecules. *Physical Chemistry Chemical Physics, 4*(7), 1093–1100. https://doi.org/10.1039/b110941n

4. Ebata, T., Minejima, C., & Mikami, N. (2002). A new electronic state of aniline observed in the transient IR absorption spectrum from S1 in a supersonic jet. *Journal of Physical Chemistry A, 106*(46), 11070–11074. https://doi.org/10.1021/jp021457t

5. Spesyvtsev, R., Kirkby, O. M., & Fielding, H. H. (2012). Ultrafast dynamics of aniline following 269–238 nm excitation and the role of the S2(π3s/$\pi\sigma^*$) state. *Faraday Discussions, 157*, 165–179. https://doi.org/10.1039/c2fd20076g

6. Spesyvtsev, R., Kirkby, O. M., Vacher, M., & Fielding, H. H. (2012). Shedding new light on the role of the Rydberg state in the photochemistry of aniline. *Physical Chemistry Chemical Physics, 14*(28), 9942–9947. https://doi.org/10.1039/c2cp41785e

7. Roberts, G. M., Williams, C. A., Young, J. D., Ullrich, S., Paterson, M. J., & Stavros, V. G. (2012). Unraveling ultrafast dynamics in photoexcited aniline. *Journal of the American Chemical Society, 134*(30), 12578–12589. https://doi.org/10.1021/ja3029729

8. Montero, R., Conde, L. P., Ovejas, V., Martnez, R., Castao, F., & Longarte, A. (2011). Ultrafast dynamics of aniline in the 294–234 nm excitation range: the role of the $\pi\sigma^*$ state. *Journal of Chemical Physics, 135*(5), 054308. https://doi.org/10.1063/1.3615544

9. Rajasekhar, B. N., Veeraiah, A., Sunanda, K., & Jagatap, B. N. (2013). Excited states of aniline by photoabsorption spectroscopy in the 30 000–90 000 cm-1 region using synchrotron radiation. *Journal of Chemical Physics, 139*(6), 064303. https://doi.org/10.1063/1.4817206

10. Thompson, J. O. F., Livingstone, R. A., & Townsend, D. (2013). Following the relaxation dynamics of photoexcited aniline in the 273–266 nm region using time-resolved photoelectron imaging. *Journal of Chemical Physics*. https://doi.org/10.1063/1.4813005

11. Roberts, G. M., & Stavros, V. G. (2014). The role of $\pi\sigma^*$ states in the photochemistry of heteroaromatic biomolecules and their subunits: Insights from gas-phase femtosecond spectroscopy. *Chemical Science, 5*(5), 1698–1722. https://doi.org/10.1039/c3sc53175a

12. Thompson, J. O., Saalbach, L., Crane, S. W., Paterson, M. J., & Townsend, D. (2015). Ultraviolet relaxation dynamics of aniline, N, N -dimethylaniline and 3,5-dimethylaniline at 250 nm. *Journal of Chemical Physics, 142*(11), 03B612_1. https://doi.org/10.1063/1.4914330

13. Kirkby, O. M., Sala, M., Balerdi, G., De Nalda, R., Bañares, L., Guérin, S., & Fielding, H. H. (2015). Comparing the electronic relaxation dynamics of aniline and d7-aniline following excitation at 272–238 nm. *Physical Chemistry Chemical Physics, 17*(25), 16270–16276. https://doi.org/10.1039/C5CP01883H

14. Cole-Filipiak, N. C., & Stavros, V. G. (2019). New insights into the dissociation dynamics of methylated anilines. *Physical Chemistry Chemical Physics, 21*(26), 14394–14406. https://doi.org/10.1039/C8CP07061J

15. Poterya, V., Nachtigallová, D., Lengyel, J., & Fárník, M. (2015). Photodissociation of aniline N-H bonds in clusters of different nature. *Physical Chemistry Chemical Physics, 17*(38), 25004–25013. https://doi.org/10.1039/C5CP04485E

16. Zawadzki, M. M., Candelaresi, M., Saalbach, L., Crane, S. W., Paterson, M. J., & Townsend, D. (2016). Observation of multichannel non-adiabatic dynamics in aniline derivatives using time-resolved photoelectron imaging. *Faraday Discussions, 194*, 185–208. https://doi.org/10.1039/C6FD00092D

17. Paterson, M. J., & Townsend, D. (2020). Rydberg-to-valence evolution in excited state molecular dynamics. *International Reviews in Physical Chemistry, 39*(4), 517–567. https://doi.org/10.1080/0144235X.2020.1815389

18. Honda, Y., Hada, M., Ehara, M., & Nakatsuji, H. (2002). Excited and ionized states of aniline: Symmetry adapted cluster configuration interaction theoretical study. *Journal of Chemical Physics, 117*(5), 2045–2052. https://doi.org/10.1063/1.1487827

19. Hou, X.-J., Quan, P., Höltzl, T., Veszprémi, T., & Nguyen, M. T. (2005). Theoretical Study of Low-Lying Triplet States of Aniline. *Journal of Physical Chemistry A, 109*, 10396–10402. https://doi.org/10.1021/jp0533527

20. Wang, F., Neville, S. P., Wang, R., & Worth, G. A. (2013). Quantum dynamics study of photoexcited aniline. *Journal of Physical Chemistry A, 117*(32), 7298–7307. https://doi.org/10.1021/jp401116c

21. Sala, M., Kirkby, O. M., Guérin, S., & Fielding, H. H. (2014). New insight into the potential energy landscape and relaxation pathways of photoexcited aniline from CASSCF and XMCQDPT2 electronic structure calculations. *Physical Chemistry Chemical Physics, 16*(7), 3122–3133. https://doi.org/10.1039/C3CP54418D

22. Ray, J., & Ramesh, S. G. (2018). Conical intersections involving the lowest $1\pi\sigma*$ state in aniline: Role of the NH2 group. *Chemical Physics, 515*, 77–87. https://doi.org/10.1016/j.chemphys.2018.03.015

23. Jhang, W. R., Lai, H. Y., Lin, Y. C., Lee, C., Lee, S. H., Lee, Y. Y., Ni, C. K., & Tseng, C. M. (2019). Triplet vs $\pi\sigma*$ state mediated N-H dissociation of aniline. *Journal of Chemical Physics, 151*(14), 141101. https://doi.org/10.1063/1.5121350

24. Ashfold, M. N. R., Cronin, B., Devine, A. L., Dixon, R. N., & Nix, M. G. D. (2006). The role of $\pi\sigma^*$ excited states in the photodissociation of heteroaromatic molecules. *Science, 312*(5780), 1637–1640. https://doi.org/10.1126/science.1125436

25. Esboui, M., & Jaidane, N. (2015). Non-radiative deactivation in phenol-pyridine complex: Theoretical study. *Photochemical and Photobiological Sciences, 14*(6), 1127–1137. https://doi.org/10.1039/C4PP00199K

26. Yeh, J. H., Shen, T. L., Nocera, D. G., Leroi, G. E., Suzuka, I., Ozawa, H., & Namuta, Y. (1996). Resonance two-photon Ionization spectroscopy of the aniline dimer. *Journal of Physical Chemistry, 100*(11), 4385–4389. https://doi.org/10.1021/jp952415q

27. Schemmel, D., & Schütz, M. (2010). Molecular aniline clusters. I. the electronic ground state. *Journal of Chemical Physics, 132*(17), 174303. https://doi.org/10.1063/1.3419505

28. Schemmel, D., & Schütz, M. (2010). Molecular aniline clusters. II. the low-lying electronic excited states. *Journal of Chemical Physics, 133*(13), 134307. https://doi.org/10.1063/1.3488227

29. Montero, R., Lamas, I., León, I., Fernández, J. A., & Longarte, A. (2019). Excited state dynamics of aniline homoclusters. *Physical Chemistry Chemical Physics, 21*(6), 3098–3105. https://doi.org/10.1039/C8CP06416D

30. Bonin, J., & Robert, M. (2011). Photoinduced proton-coupled electron transfers in biorelevant phenolic systems. *Photochemistry and Photobiology, 87*(6), 1190–1203. https://doi.org/10.1111/j.1751-1097.2011.00996.x

31. Weinberg, D. R., Gagliardi, C. J., Hull, J. F., Murphy, C. F., Kent, C. A., Westlake, B. C., Paul, A., Ess, D. H., McCafferty, D. G., & Meyer, T. J. (2012). Proton-coupled electron transfer. In *Chemical Reviews* (Vol. 112, Issue 7, pp. 4016–4093). doi:https://doi.org/10.1021/cr200177j

32. Mayer, J. M., Hrovat, D. A., Thomas, J. L., & Borden, W. T. (2002). Proton-Coupled Electron Transfer versus Hydrogen Atom Transfer in Benzyl/Toluene, Methoxyl/Methanol, and Phenoxyl/ Phenol Self-Exchange Reactions. *Journal of the American Chemical Society, 124*, 11142–11147. https://doi.org/10.1021/ja012732c

33. Tishchenko, O., Truhlar, D. G., Ceulemans, A., & Minh, T. N. (2008). A unified perspective on the hydrogen atom transfer and proton-coupled electron transfer mechanisms in terms of topographic features of the ground and excited potential energy surfaces as exemplified by the reaction between phenol and radicals. *Journal of the American Chemical Society, 130*(22), 7000–7010. https://doi.org/10.1021/ja7102907

34. Ahlrichs, R., Bär, M., Häser, M., Horn, H., & Kölmel, C. (1989). Electronic structure calculations on workstation computers: The program system turbomole. *Chemical Physics Letters, 162*(3), 165–169. https://doi.org/10.1016/0009-2614(89)85118-8

35. Weigend, F., Häser, M., Patzelt, H., & Ahlrichs, R. (1998). RI-MP2: Optimized auxiliary basis sets and demonstration of efficiency. *Chemical Physics Letters, 294*(1–3), 143–152. https://doi.org/10.1016/S0009-2614(98)00862-8

36. Hättig, C. (2003). Geometry optimizations with the coupled-cluster model CC2 using the resolution-of-the-identity approximation. *Journal of Chemical Physics, 118*(17), 7751–7761. https://doi.org/10.1063/1.1564061

37. Köhn, A., & Hättig, C. (2003). Analytic gradients for excited states in the coupled-cluster model CC2 employing the resolution-of-the-identity approximation. *Journal of Chemical Physics, 119*(10), 5021–5036. https://doi.org/10.1063/1.1597635

38. Rutledge, L. R., Navarro-Whyte, L., Peterson, T. L., & Wetmore, S. D. (2011). Effects of extending the computational model on DNA-protein T-shaped interactions: The case of adenine-histidine dimers. *Journal of Physical Chemistry A, 115*(45), 12646–12658. https://doi.org/10.1021/jp203248j

39. Kadam, R. U., Garg, D., Schwartz, J., Visini, R., Sattler, M., Stocker, A., Darbre, T., & Reymond, J. L. (2013). CH-π "t-shape" interaction with histidine explains binding of aromatic galactosides to Pseudomonas aeruginosa lectin LecA. *ACS Chemical Biology, 8*(9), 1925–1930. https://doi.org/10.1021/cb400303w

40. Nishio, M., Umezawa, Y., Fantini, J., Weiss, M. S., & Chakrabarti, P. (2014). CH-π hydrogen bonds in biological macromolecules. In *Physical Chemistry Chemical Physics* (Vol. 16, Issue 25, pp. 12648–12683). doi:https://doi.org/10.1039/C4CP00099D

41. Tsuzuki, S., & Fujii, A. (2008). Nature and physical origin of CH/π interaction: Significant difference from conventional hydrogen bonds. *Physical Chemistry Chemical Physics, 10*(19), 2584–2594. https://doi.org/10.1039/b718656h

42. Sinnokrot, M. O., & Sherrill, C. D. (2004). Substituent effects in π-π interactions: Sandwich and t-shaped configurations. *Journal of the American Chemical Society, 126*(24), 7690–7697. https://doi.org/10.1021/ja049434a

43. Smith, T., Slipchenko, L. V., & Gordon, M. S. (2008). Modeling π-π interactions with the effective fragment potential method: The benzene dimer and substituents. *Journal of Physical Chemistry A, 112*(23), 5286–5294. https://doi.org/10.1021/jp800107z

44. Ashfold, M. N. R., King, G. A., Murdock, D., Nix, M. G. D., Oliver, T. A. A., & Sage, A. G. (2010). πσ* Excited states in molecular photochemistry. *Physical Chemistry Chemical Physics, 12*(6), 1218–1238. https://doi.org/10.1039/B921706A

45. Scheiner, S. (2000). Theoretical studies of excited state proton transfer in small model systems. *Journal of Physical Chemistry A, 104*(25), 5898–5909. https://doi.org/10.1021/jp000125q

46. Sobolewski, A. L., & Domcke, W. (1999). Ab initio potential-energy functions for excited state intramolecular proton transfer: A comparative study of o-hydroxybenzaldehyde, salicylic acid and 7-hydroxy-1-indanone. *Physical Chemistry Chemical Physics, 1*(13), 3065–3072. https://doi.org/10.1039/a902565k

47. Sobolewski, A. L., & Domcke, W. (2000). Photoinduced charge separation in indole-water clusters. *Chemical Physics Letters, 329*(1–2), 130–137. https://doi.org/10.1016/S0009-2614(00)00983-0

48. Sobolewski, A. L., & Domcke, W. (2001). Photoinduced electron and proton transfer in phenol and its clusters with water and ammonia. *Journal of Physical Chemistry A, 105*(40), 9275–9283. https://doi.org/10.1021/jp011260l

49. Tanaka, H., & Nishimoto, K. (1984). Ab initio molecular orbital study on the electronic structure of some excited hydrogen-bonding systems. *Journal of Physical Chemistry, 88*(6), 1052–1055. https://doi.org/10.1021/j150650a002

50. Ikeda, N., Okada, T., & Mataga, N. (1980). Fluorescence and picosecond laser photolysis studies on the deactivation processes of excited hydrogen bonding systems. *Chemical Physics Letters, 69*(2), 251–254. https://doi.org/10.1016/0009-2614(80)85057-3

51. Martin, M. M., Ikeda, N., Okada, T., & Mataga, N. (1982). Picosecond laser photolysis studies of deactivation processes of excited hydrogen-bonding complexes. 2. Dibenzocarbazole-pyridine systems. *Journal of Physical Chemistry, 86*(21), 4148–4156. https://doi.org/10.1021/j100218a012

52. Martin, M., Miyasaka, H., Karen, A., & Mataga, N. (1985). Charge transfer in dibenzocarbazole-pyridine hydrogen-bonded complexes: The role of the geometry of the complex. *Journal of Physical Chemistry, 89*(1), 182–185. https://doi.org/10.1021/j100247a038

53. Ikeda, N., Miyasaka, H., Okada, T., & Malaga, N. (1983). Picosecond Laser Photolysis Studies of Deactivation Processes of Excited Hydrogen Bonding Complexes. 3. Detection of the Nonfluorescent Charge-Transfer State in the Excited 1-Aminopyrene-Pyridine Hydrogen Bonded Pair and Related Systems†. *Journal of the American Chemical Society, 105*(16), 5206–5211. https://doi.org/10.1021/ja00354a004

54. Miyasaka, H., Tabata, A., Ojima, S., Ikeda, N., & Mataga, N. (1993). Femtosecond-picosecond laser photolysis studies on the mechanisms of fluorescence quenching induced by hydrogen-bonding interactions - 1-Pyrenol-pyridine systems. *Journal of Physical Chemistry, 97*(31), 8222–8228. https://doi.org/10.1021/j100133a017

55. Mataga, N., & Miyasaka, H. (2007). Electron Transfer and Exciplex Chemistry. In *Advances in Chemical Physics* (pp. 431–496). John Wiley & Sons, Ltd. doi:https://doi.org/10.1002/9780470141663.ch8

56. Herbich, J., Kijak, M., Zielińska, A., Thummel, R. P., & Waluk, J. (2002). Fluorescence quenching by pyridine and derivatives induced by intermolecular hydrogen bonding to pyrrole-containing heteroaromatics. *Journal of Physical Chemistry A, 106*(10), 2158–2163. https://doi.org/10.1021/jp012515y

57. Waluk, J. (2003). Hydrogen-Bonding-Induced Phenomena in Bifunctional Heteroazaaromatics. *Accounts of Chemical Research, 36*(11), 832–838. https://doi.org/10.1021/ar0200549

58. Rode, M. F., & Sobolewski, A. L. (2008). Photophysics of inter- and intra-molecularly hydrogen-bonded systems: Computational studies on the pyrrole-pyridine complex and 2(2′-pyridyl)pyrrole. *Chemical Physics, 347*(1–3), 413–421. https://doi.org/10.1016/j.chemphys.2007.11.013

59. Omidyan, R., Salehi, M., & Azimi, G. (2015). A theoretical exploration of the nonradiative deactivation of hydrogen-bond complexes: Isoindole-pyridine and quinoline-pyrrole. *RSC Advances, 5*(118), 97619–97628. https://doi.org/10.1039/C5RA18950K